

RESEARCH ARTICLE

A novel imidazolinone metformin-methylglyoxal metabolite promotes endothelial cell angiogenesis via the eNOS/HIF-1 α pathway

Huong Nguyen¹ | Jia Yi Koh¹ | Hainan Li¹ | Argel Islas-Robles² |
Sai Pranathi Meda Venkata¹ | Jie-Mei Wang^{1,3} | Terrence J. Monks¹

¹Department of Pharmaceutical Sciences, Eugene Applebaum College of Pharmacy and Health Sciences, Wayne State University, Detroit, MI, USA

²Institute for In vitro Science Inc., Gaithersburg, MD, USA

³Centers for Molecular Medicine and Genetics, Wayne State University, Detroit, MI, USA

Correspondence

Terrence J. Monks and Jie-Mei Wang, Department of Pharmaceutical Sciences, Eugene Applebaum College of Pharmacy & Health Sciences, Wayne State University, Address: 259 Mack Ave, 5146 Applebaum Building, Detroit, MI 48201, USA. Email: terrence.monks@wayne.edu (T. J. M.) and jiemei.wang@wayne.edu (J.-M. W.)

Funding information

This work was supported in part by NIH/NIDDK R01 DK109036 (To JMW), R01 DK119222 (To TJM and JMW) and Wayne State University new faculty startup funding in the Department of Pharmaceutical Sciences (To TJM)

Abstract

Peripheral arterial disease (PAD) is one of the major complications of diabetes due to an impairment in angiogenesis. Since there is currently no drug with satisfactory efficacy to enhance blood vessel formation, discovering therapies to improve angiogenesis is critical. An imidazolinone metabolite of the metformin-methylglyoxal scavenging reaction, (*E*)-1,1-dimethyl-2-(5-methyl-4-oxo-4,5-dihydro-1*H*-imidazol-2-yl) guanidine (IMZ), was recently characterized and identified in the urine of type-2 diabetic patients. Here, we report the pro-angiogenesis effect of IMZ (increased aortic sprouting, cell migration, network formation, and upregulated multiple pro-angiogenic factors) in human umbilical vein endothelial cells. Using genetic and pharmacological approaches, we showed that IMZ augmented angiogenesis by activating the endothelial nitric oxide synthase (eNOS)/hypoxia-inducible factor-1 alpha (HIF-1 α) pathway. Furthermore, IMZ significantly promoted capillary density in the in vivo Matrigel plug angiogenesis model. Finally, the role of IMZ in post-ischemic angiogenesis was examined in a chronic hyperglycemia mouse model subjected to hind limb ischemia. We observed improved blood perfusion, increased capillary density, and reduced tissue necrosis in mice receiving IMZ compared to control mice. Our data demonstrate the pro-angiogenic effects of IMZ, its underlying mechanism, and provides a structural basis for the development of potential pro-angiogenic agents for the treatment of PAD.

KEYWORDS

angiogenesis, endothelial nitric oxide synthase, hypoxia-inducible factor-1 alpha, methylglyoxal, metformin

Abbreviations: bFGF, basic fibroblast growth factor; DAF-FM DA, 4-amino-5-methylamino-2',7'-difluorofluorescein diacetate; EC, endothelial cells; eIF-4E, eukaryotic translation initiation factor 4E; eNOS, endothelium nitric oxide synthase; HB-EGF, heparin-binding epidermal growth factor; HIF-1 α , hypoxia-inducible factor 1 alpha; HUVECs, human umbilical vein endothelial cells; IGFBP-2, insulin-like growth factor binding protein 2; IMZ, (*E*)-1,1-dimethyl-2-(5-methyl-4-oxo-4,5-dihydro-1*H*-imidazol-2-yl)guanidine; MG, methylglyoxal; NO, nitric oxide; PAD, peripheral artery disease; PDGF-AB, platelet-derived growth factor AB; PI3K, phosphatidylinositol 3-kinase; STZ, streptozotocin; VEGF, vascular endothelial growth factor; WT, wild type.

This is an open access article under the terms of the Creative Commons Attribution-NonCommercial-NoDerivs License, which permits use and distribution in any medium, provided the original work is properly cited, the use is non-commercial and no modifications or adaptations are made.

© 2021 The Authors. *The FASEB Journal* published by Wiley Periodicals LLC on behalf of Federation of American Societies for Experimental Biology

1 | INTRODUCTION

Peripheral artery disease (PAD) is one of the most devastating complications of diabetes.¹ PAD is associated with heart failure and stroke.¹ In severe cases, PAD causes critical limb ischemia (CLI), which can lead to limb amputation.¹ The primary treatment for severe PAD and CLI is revascularization.² However, a significant proportion of patients with CLI are either unsuitable or have failed revascularization.³ Therapeutic angiogenesis, aiming to promote blood vessel growth from existing vasculature and thus increase blood flow to ischemic tissues, has emerged as an alternative therapy for PAD/CLI.⁴ However, clinical translation of current approaches of using genes, proteins, and cells has been challenging for multiple reasons such as short protein half-life, vector-limiting toxicity, and poor pharmacokinetic profiles.⁵ Therefore, discovering novel therapies with the focus on small molecules is of significant interest in the field.

Methylglyoxal (MG) is a reactive dicarbonyl generated during glycolysis in the presence of high glucose and oxidative stress and is elevated in the plasma of patients with diabetes mellitus. MG is recognized as a significant contributor to cellular damage and dysfunction during diabetic vascular complications.⁶ The first line anti-hyperglycemic drug, metformin, is a scavenger of MG.⁷ Our group has recently identified and characterized a novel imidazolinone metabolite produced by the metformin-MG reaction, (*E*)-1,1-dimethyl-2-(5-methyl-4-oxo-4,5-dihydro-1*H*-imidazol-2-yl)guanidine (IMZ) (Figure S1).⁸ We have determined that the urine IMZ levels are between 18.8 nM to 4.3 μ M in diabetic patients receiving metformin.⁸ Because IMZ contains an imidazolinone/guanidine group, it has structural similarities to many pharmacologically active compounds known to increase nitric oxide (NO) production and endothelial cell (EC) function, such as moxonidine, agmatine, and arginine.⁹⁻¹¹ However, whether IMZ regulates angiogenesis is unknown.

Hypoxia-inducible factor-1 alpha (HIF-1 α) is an oxygen-dependent transcriptional activator.¹² HIF-1 α induces the transcription of more than 60 genes, including vascular endothelial growth factor (VEGF) and basic fibroblast growth factor (bFGF), which regulate immunological responses, vascularization, and anaerobic metabolism.¹² In the endothelium, HIF-1 α plays a crucial role in maintaining EC angiogenesis.¹³ Loss of HIF-1 α inhibits many essential EC function features, including network formation, migration, wound healing, and blood vessel growth.¹⁴ The stability and activity of HIF-1 α are regulated by oxygen-dependent and -independent mechanisms. Various growth factors and cytokines increase HIF-1 α levels independent of oxygen concentration, with phosphatidylinositol 3-kinase (PI3K)/AKT being the most common pathway.¹⁵ Of particular note, NO stabilizes HIF-1 α under normoxic conditions via inhibition of

HIF-1 α hydroxylation.¹⁶ To date, the mechanisms of HIF-1 α up-regulation are not fully understood.

Herein, we examined the effects of IMZ on EC angiogenesis using in-vitro functional assays (aortic sprouting assay, network formation, migration, and proliferation assay), an in vivo Matrigel plug assay, and ischemia-induced angiogenesis in animals with chronic hyperglycemia. We also investigated potential mechanisms by which HIF-1 α and endothelial nitric oxide synthase (eNOS) participate in IMZ-induced augmentation of EC angiogenesis. Data generated from this study have revealed the pro-angiogenic properties of IMZ, intracellular signaling pathway(s) engaged by IMZ, and the structural basis of IMZ in the development of potential therapeutics for PAD.

2 | RESEARCH DESIGN AND METHODS

2.1 | IMZ synthesis

IMZ was synthesized and the structure confirmed by NMR and LC-MS/MS analysis as described previously (Figures S2 and S3).⁸

2.2 | Animals and cell culture

Male C57B/6J mice (8-12 weeks old) were purchased from Jackson Laboratory. All animal experiments were performed according to Wayne State University Institutional Animal Care and Use Committee guidelines. The primary human umbilical vein endothelial cells (HUVECs) from four different donors were obtained from the American Type Culture Collection. Cells were grown in vascular cell basal media (VCBM) supplemented with Vasculife VEGF LifeFactors Kit (Lifeline Cell Technology). Only cells between passages 2 to 5 were used for experiments.

2.3 | Matrigel network formation assay

The angiogenic activity of endothelial cells was examined using an in vitro network formation assay, as previously described.¹⁷ Each well of 48-well plates were coated with 160 μ L of growth factor-reduced phenol-red free extracellular matrix gel, Matrigel (Corning Incorporated). HUVECs were cultured on prepared Matrigel at a density of 50 000 cells/well with the 10% FBS- basal media containing IMZ at a final concentration of 1 nM-1 μ M. Subsequently, the cells were incubated at 37°C, 5% CO₂ for 16 h. Network formation was examined by phase-contrast microscopy (EVOS, Thermo Fisher Scientific) and accumulated network length

was quantified at five random fields per well using ImageJ software (National Institutes of Health). Five images were taken at five random fields per sample to cover most of the area in the well. The network length was calculated based on the average value of five images within one sample. The experiment was conducted four times using four donors of HUVECs.

2.4 | Modified Boyden chamber migration assay

Migration assays were performed in Boyden chambers (Transwell Costar, 6.5 mm diameter, 8 μ m pore size) according to the manufacturer's instructions. Briefly, the inserts were coated with 7.5 μ g/cm² collagen type I (Corning Incorporated) for 2 h. HUVECs (3×10^4 cells) in serum-free medium containing IMZ or vehicle control were plated onto the top of each chamber insert and 10% FBS-medium was added to the bottom chamber as migration stimuli. After 16 h of incubation at 37°C, in 5% CO₂, the inserts were removed; un-migrated cells were wiped off by wet cotton. Cells that migrated to the bottom portion of the inserts were fixed with 4% paraformaldehyde and stained with 0.5% crystal violet. Cell numbers were counted using an inverted microscope at 20 \times objective lens at four random fields/insert. The number of migrated cells was calculated based on the average value of four images taken at four random fields per sample. The experiment was conducted four times using four donors of HUVECs.

2.5 | Cell proliferation assay

Endothelial cell proliferation was evaluated using the BrdU cell proliferation assay kit (Cell Signaling, #6813) according to the manufacturer's instructions. Briefly, endothelial cells were plated on a 96 well plate and treated with IMZ (1 μ M) or vehicle control for 24 h in basal medium supplemented with 10% FBS, following by 16-h incubation with BrdU. The experiment was conducted four times using four donors of HUVECs.

2.6 | Measurement of NO production

NO production was semi-quantified using the NO-sensitive fluorescence dye, DAF-FM DA (Thermo Fisher Scientific). Briefly, serum-starved HUVECs were first loaded with DAF-FM DA (1 μ M) for 15 min at 37°C. Subsequently, cells were gently washed twice with PBS. HUVECs were treated with 1 μ M IMZ for 20 min. Next, the cells were washed with PBS and fixed with 4% paraformaldehyde. The fluorescence

of the NO-sensitive dye was examined by fluorescence microscopy (EVOS, Thermo Fisher Scientific) and quantified by ImageJ.

2.7 | Western blot analyses

Procedures were performed as previously described.¹⁸ Briefly, after 24-h treatment of IMZ (1 μ M) or vehicle control in basal medium supplemented with 10% FBS, cells were washed with ice-cold PBS and lysed with cell lysate buffer (Cell Signaling), containing 1 mM Pefabloc SC, cOmplete protease inhibitor cocktail, and PhosSTOP phosphatase inhibitor cocktail (Roche). Equal amounts of denatured proteins (40 μ g) were separated by 8%-14% polyacrylamide gel electrophoresis (SDS-PAGE) and transferred to PVDF membranes for immunoblotting using antibodies directed against the protein targets as described in Table S1. Blots were imaged with the Odyssey Fc imaging system (Li-Cor). Densitometric analysis was performed using Image Studio Lite software (Li-Cor).

2.8 | Quantitative RT-PCR

Total RNA was extracted using the RNeasy Mini Kit (Qiagen) following the manufacturer's instructions. Complementary deoxyribonucleic acid (cDNA) was synthesized from 100 ng of total RNA using a High Capacity cDNA reverse transcription kit (Thermo Fisher Scientific). The cDNA template was mixed with HIF-1 α PCR primers, SYBR green PCR master mix (Thermo Fisher Scientific) and run in LightCycler 480 Software 1.5. Gene expression was normalized against the internal control, GAPDH. Table S2 includes the primer sequences.

2.9 | Small interfering RNA transfection

HUVECs at 70%-80% confluence were transfected with lipofectamine 2000 (Invitrogen) and human HIF-1 α siRNA or scrambled siRNA (Santa Cruz) following the manufacturer's instructions. Specific knockdown of targeted protein was confirmed by western blot. A similar protocol was used for eNOS siRNA transfection.

2.10 | Human pro-angiogenic protein array

The Proteome Profiler Human Angiogenesis Array (R&D Systems, #ARY007) was performed following the manufacturer's instructions. Briefly, HUVECs at 80% confluence were treated with IMZ (1 μ M) or vehicle control (water) for

24 h. The membrane, spotted with 55 angiogenesis-related antibodies, was blocked for 1 h at room temperature. Cell lysates (200 µg) were mixed with a cocktail of biotinylated detection antibodies (15 µL), and added to the membrane, and incubated overnight at 4°C. Membranes were exposed to streptavidin-horseradish peroxidase for 30 min, followed by chemiluminescence detection reagents, and exposed for 10 min. The intensity of protein expression was quantified with the Odyssey Fc imaging system (Li-Cor). The protein array map can be found at <https://resources.rndsystems.com/pdfs/datasheets/ary007.pdf>.

2.11 | Subcutaneous Matrigel plug assay

Matrigel plug assay for evaluation of angiogenesis in-vivo was performed as described.^{19,20} Mice were injected subcutaneously, using a 24G needle, with ice-cold Matrigel (BD Biosciences) supplemented with IMZ 1 µM or vehicle control (water). The resulting mixture solidified to form a plug upon implantation. On day 14, the mice were euthanized. Plugs were removed and fixed with 4% formaldehyde at 4°C for 12 h, and embedded in OCT.

2.12 | Hind limb ischemic surgery and laser Doppler blood perfusion imaging

Adult male C57BL/6 mice were rendered hyperglycemic by low-dose injections of streptozotocin (STZ) at 50 mg/kg for five consecutive days. Control (WT) mice received citrate buffer injections. Upon development of hyperglycemia (≥ 250 mg/dL glucose), the animals were housed for at least another 3 months. Both WT and STZ mice received hind limb ischemia surgery, and were then randomly divided into 4 groups: WT + PBS, WT + IMZ (20 mg/kg, ip, twice/day), STZ + PBS, STZ + IMZ (20 mg/kg, ip, twice/day). Hind limb ischemia was induced as described.²¹ After isolation from nerves and vein, the proximal and distal portions of the femoral artery and saphenous artery were ligated with 6-0 silk suture. All arterial branches between the ligation were obliterated. The skin was closed with 4-0 nylon suture. Sham surgery was conducted in the same manner, although the blood vessels were not ligated. The mice were given analgesics (Buprenorphine, 1 mg/kg SC, before and 72 h after the surgery) and postoperative antibiotics (ticarcillin, 50 mg/kg, IP, for 3 days). In the hind limb ischemic study, mice were given the first dose of IMZ (20 mg/kg body weight, ip injection) immediately after the surgery. Subsequently, the animals received IMZ at the dose of 20 mg/kg, twice a day, for 21 days post-surgery. Blood flow was measured using a Laser Doppler and PeriScan PIM 3 System (Perimed). To avoid the interference induced by the slight variations of

temperature and the depth of anesthesia, we presented the recovery index as the ratio of blood flow in the ischemic paw to sham paw. At the end of the experiments, hind limb muscles were harvested for immunofluorescence studies.

2.13 | Immunofluorescence staining

Matrigel plugs or muscles were collected, fixed with 4% paraformaldehyde, and embedded in OCT. 8 µm (muscle) and 10 µm (Matrigel plugs) sections were cut using a cryostat and immediately transferred to poly-L-lysine coated slides. Permeabilization buffer containing 1% BSA and 0.4% Triton X-100 in PBS was used to permeabilize tissue. Non-specific binding was blocked by incubating the tissue sections with 3% BSA in PBS-T for 30 min at room temperature. Tissue sections were then incubated with a goat anti-mouse CD31 antibody (R&D, #AF3628) overnight in a humidified chamber, followed by Donkey anti-goat green IgG NorthernLights NL493-conjugated secondary Antibody (R&D system, #NL-493). Sections were mounted with ProLong Gold Antifade Mountant with DAPI (Invitrogen). Fluorescence images were recorded on three random fields per section with an EVOS FL auto inverted microscope (Life Technologies).

2.14 | Statistical analysis

All data were analyzed using GraphPad Prism 7 software and presented as mean \pm standard deviation (SD). Statistical differences between 2 groups were determined with the Mann-Whitney nonparametric test. For a comparison of more than two groups, one-way ANOVA with Tukey's multiple comparison test was used for analysis. For laser Doppler blood perfusion data, two-way repeated-measures ANOVA followed by Bonferroni's multiple comparison test was used. A *P*-value of less than .05 was considered statistically significant.

3 | RESULTS

3.1 | IMZ increases EC mediated angiogenesis in vitro

The structure of the product formed during the reaction between metformin and methylglyoxal (Figure S1) was confirmed as IMZ by NMR and LC-MS/MS analysis (Figures S2 and S3) as previously described.⁸ To characterize the effects of IMZ on each aspect of the endothelial mediated angiogenic processes, functional tests, including network formation on Matrigel, migration (Transwell), and proliferation (BrdU assay) were performed. Since plasma levels of

IMZ in diabetic patients remains unknown, we employed a range of IMZ (nM to μ M) based on IMZ concentrations detected in urine samples.⁸ IMZ at a concentration as low as 1 nM increased network length \sim 30% compared to control (Figure 1A,B). The maximum effect of IMZ on network formation was seen in HUVECs treated with IMZ at 1 μ M. In addition, IMZ at 1 μ M, but not lower concentrations, increased the capacity of HUVECs to migrate through a collagen-coated membrane in the Boyden chamber assay (Figure 1C,D). Interestingly, IMZ still significantly increased the number of cells migrating through the pore when IMZ was placed in the lower chamber, suggesting that IMZ might possess chemotactic properties (Figure S4). In contrast, IMZ did not affect endothelial cell proliferation as there was no difference between IMZ and control treatments in the BrdU proliferation assay (Figure 1E). Together, these data suggest that IMZ at remarkably low concentrations significantly increases EC-mediated angiogenesis.

3.2 | IMZ increases pro-angiogenic factor expression in HUVECs

As IMZ induced EC angiogenesis, we next determined the effect of IMZ on the secretion of angiogenic factors. Using

a comparative proteome profiler array of 55 different angiogenesis mediators, we found that IMZ (1 μ M) significantly increased the expression of several intracellular and secreted pro-angiogenic factors, including vascular endothelial growth factor (VEGFA, \sim 70% vs control), basic fibroblast growth factor (bFGF, \sim 50% vs control), platelet-derived growth factor AB (PDGF-AB, \sim 60% vs control) and insulin-like growth factor binding protein 2 (IGFBP-2, \sim 75% vs control) (Figure 2A,B). The IMZ mediated increases of VEGFA and bFGF were further validated by western blot analysis since the roles of these two factors in EC mediated angiogenesis are the most well established.²² IMZ (1 μ M) significantly increased monomer and dimer versions of VEGFA and bFGF expression compared to control (Figure 2C). Furthermore, our data showed that IMZ did not affect the expression of other VEGF family members, such as VEGFB and VEGFC, as there was no statistical difference in the levels of these two VEGF family members between IMZ and control-treated HUVECs (Figure S5A). Interestingly, concomitant with the increase in VEGFA expression, IMZ tended to increase the phosphorylation of VEGF receptor 2 (VEGFR2) at Tyrosine 1059 compared to vehicle controls ($P = .0571$) (Figure S5A). Whether this trend of increased phosphorylation of VEGFR2 is directly modulated by IMZ or occurs in response to the increased VEGFA under IMZ treatment requires further investigations.

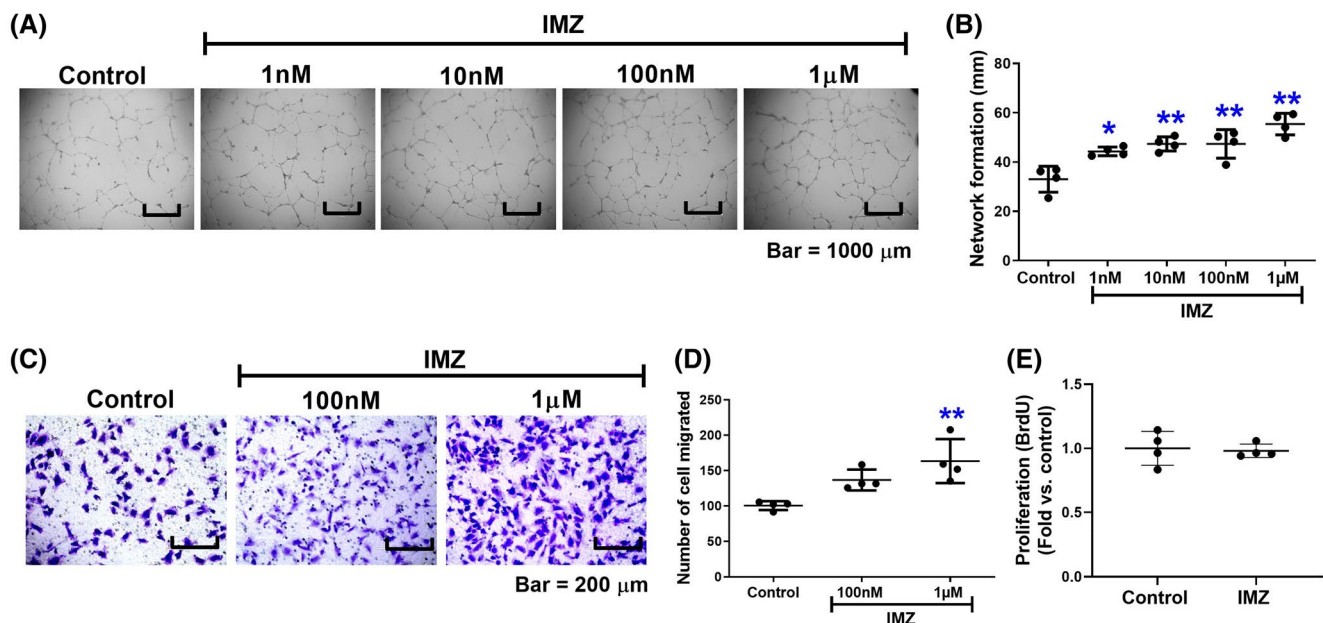


FIGURE 1 IMZ increases endothelial cell-mediated angiogenesis. A, Representative images from the network formation assay. HUVECs were cultured in growth factor reduced Matrigel in the absence or presence of different concentrations of IMZ (1 nM – 1 μ M) for 16 h. Images were acquired at a magnification of 4 \times . Bar = 1000 μ m. n = 4 per group. B, Dot-plot graph of network length derived from the network formation assay. Network length was quantified by ImageJ software. * $P < .05$ vs control, ** $P < .01$ vs control. C, Representative images from the modified Boyden chamber assay. HUVECs were treated with IMZ 100 nM or IMZ 1 μ M for 16 h. Images were acquired at a magnification of 20 \times . Bar = 200 μ m. n = 4 per group. D, Dot-plot graph of the number of cells migrating through the membrane. ** $P < .01$ vs control. E, Dot-plot graph from the proliferation assay. HUVECs were treated with IMZ (1 μ M) for 24 h; cell proliferation was evaluated with a BrdU cell proliferation assay kit. n = 4 per group. All data are presented as mean \pm SD. The statistical significance of the difference among treatments in each figure was determined by one-way ANOVA with Tukey's multiple comparison test

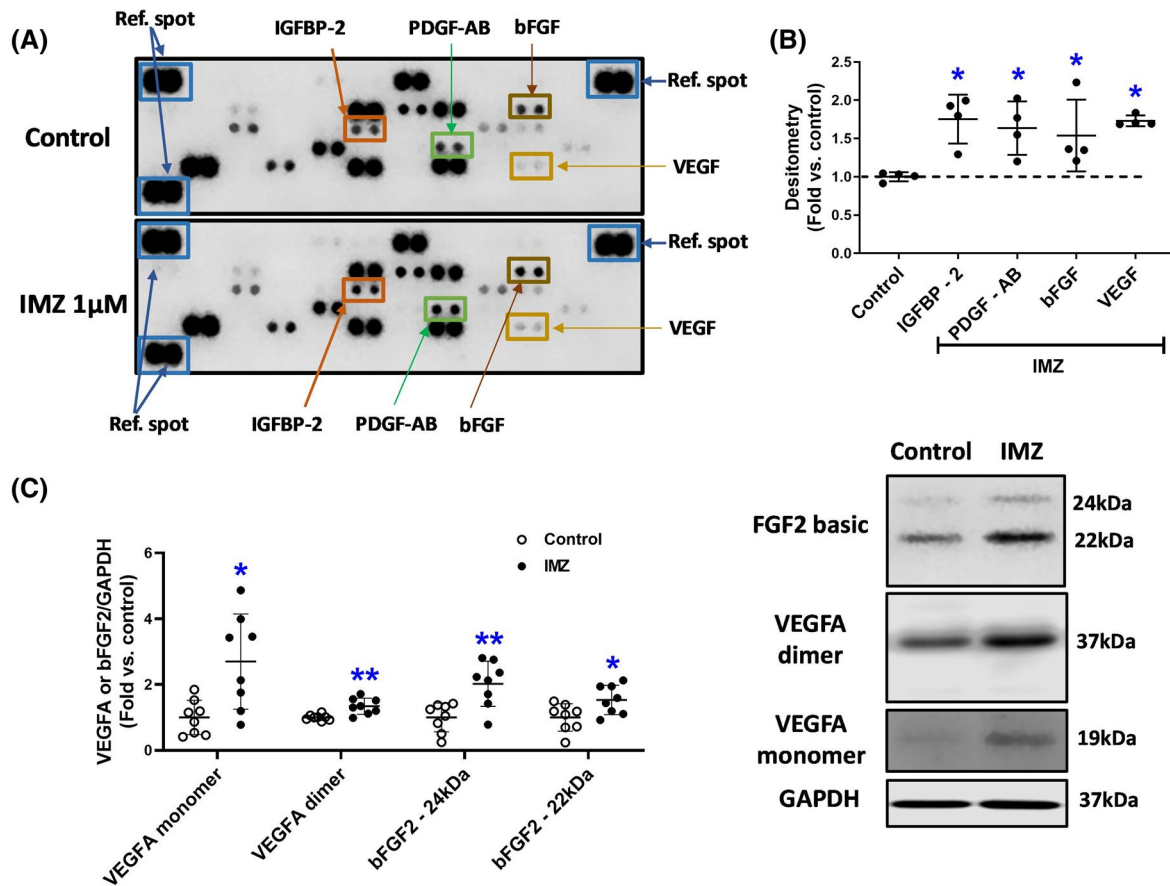


FIGURE 2 IMZ increases pro-angiogenesis mediators in HUVECs. A, Representative images from the proteome profiler human angiogenesis array from HUVECs treated with water (vehicle control, top panel) or IMZ 1 μ M (bottom panel) for 24 h. $n = 4$ per group. Ref. spots, reference spots. The unlabeled dots represent other angiogenic mediators that did not show a statistical difference between IMZ and control treatment in our analysis. B, Dot-plot graph from the densitometric analysis of selected angiogenesis mediators generated by quantifying the mean spot pixel densities from the array membrane using Image Studio Lite software. $*P < .05$ vs. control. C, Representative images from the Western blot and densitometric analysis of VEGFA and bFGF in either vehicle control HUVECs or those treated with IMZ 1 μ M for 24 h. $n = 8$ per group. $*P < .05$ vs. control, $**P < .01$ vs. control. All data are presented as mean \pm SD. The statistical significance of the difference between the two groups in each figure was determined by the Mann-Whitney test

Together, these data indicate that IMZ increases the expression of several EC-derived angiogenic factors.

3.3 | HIF-1 α is crucial for IMZ-induced angiogenesis in HUVECs

Since IMZ increased EC mediated angiogenesis and pro-angiogenic factors in HUVECs, we next examined the potential signaling pathway(s) mediating these effects. HIF-1 α is a potent activator of angiogenic signaling pathways.¹³ HIF-1 α induces the expression of numerous growth factors, including VEGFA and bFGF.¹² Because HIF-1 α was not included in the angiogenesis proteome profiler, we assessed HIF-1 α protein levels in IMZ-treated EC samples by Western blot. IMZ (1 μ M) significantly increased HIF-1 α protein level \sim 45% compared to equivalent controls (Figure 3A). In contrast, there was no difference

in HIF-1 α mRNA levels between IMZ treated and control cells, as determined by qPCR (Figure 3B), suggesting that the IMZ-induced increases in HIF-1 α protein level occurred at the post-translational level. We subsequently used an inhibitor of protein synthesis (cycloheximide, CHX) to determine if IMZ affects HIF-1 α protein degradation. HUVECs were co-treated with CHX and IMZ for 24 h. Cell lysates were harvested for HIF-1 α protein measurement by Western blot. Higher levels of HIF-1 α protein were observed in IMZ-treated HUVECs compared to control HUVECs (Figure 3C), suggesting that IMZ delayed HIF-1 α protein degradation. In addition, immunofluorescence staining revealed that IMZ significantly induces HIF-1 α nuclear translocation (Figure 3G). Furthermore, IMZ does not affect HIF-1 α phosphorylation or protein levels of HIF-2 α (Figure S5B). To investigate whether HIF-1 α has a functional role in IMZ-induced angiogenesis, HIF-1 α was knocked down using an RNA-interference approach.

HUVECs were transfected with siRNA for HIF-1 α , or with scrambled siRNA and subsequently treated with IMZ (1 μ M) for 24 h. The successful knockdown of HIF-1 α , to ~60% of control, was confirmed by Western blot (Figure 3D). EC functional tests, including migration and network formation assay, were performed on HIF-1 α siRNA transfected

cells. The enhanced migration (Figure 3E) and network formation (Figure 3F) induced by IMZ was significantly attenuated by HIF-1 α siRNA. Furthermore, in HIF-1 α deficient cells, the effects of IMZ on the increased VEGFA and FGF expression were completely blunted, suggesting that HIF-1 α plays a crucial role in IMZ-mediated VEGFA

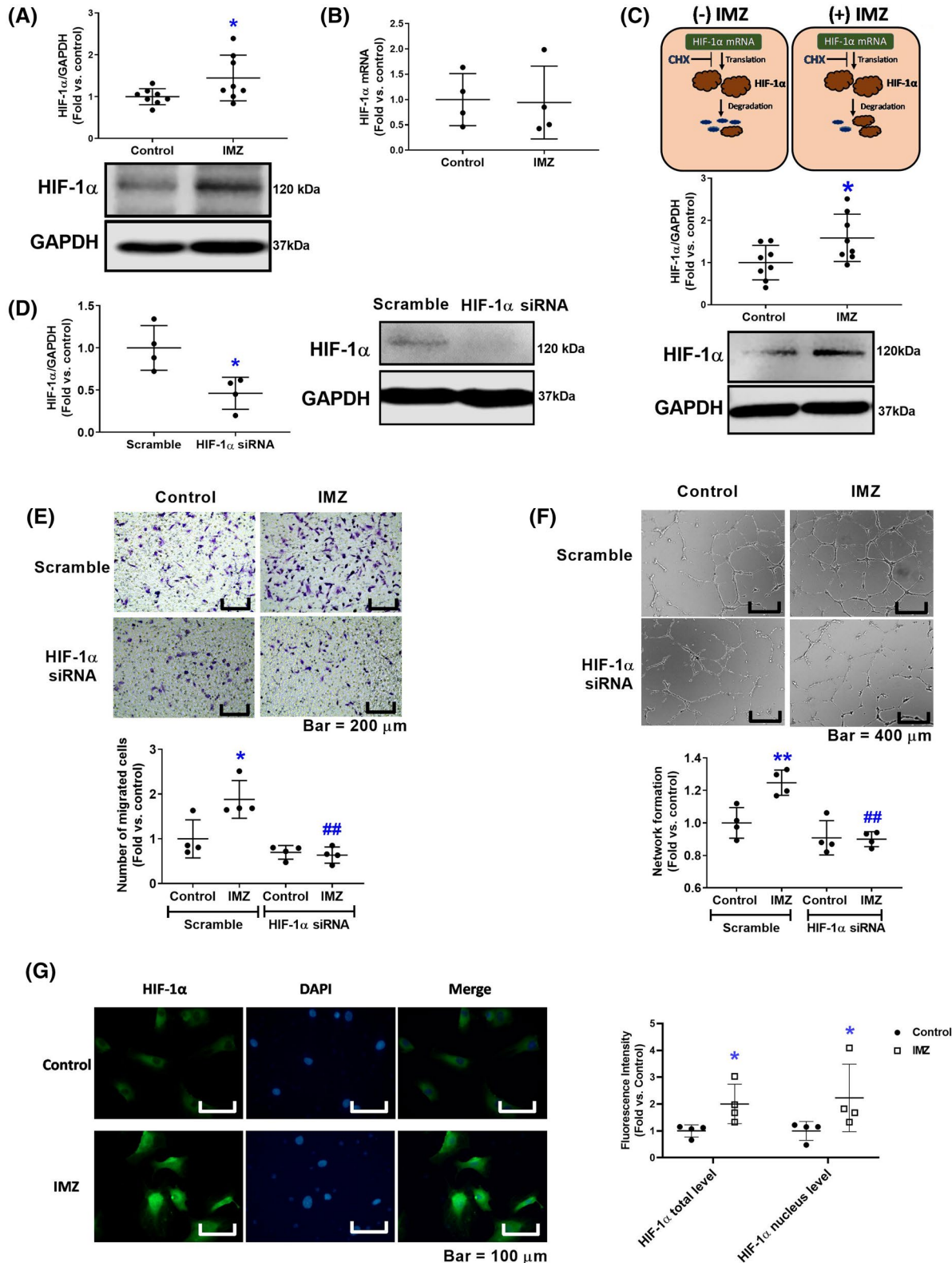


FIGURE 3 HIF-1 α plays a crucial role in IMZ-mediated angiogenesis in HUVECs. A, Western blot images and densitometric analysis of HIF-1 α in HUVECs treated with vehicle control (water) or IMZ 1 μ M for 24 h. n = 8 per group. * P < .05 vs control. B, Quantitative real-time PCR (qPCR) analysis of HIF-1 α mRNA level in the vehicle (water) control or IMZ 1 μ M treated HUVECs. GAPDH was used as an internal loading control. n = 4 per group. C, Schema, Western blot images, and densitometric analysis comparing HIF-1 α protein level in the presence of the protein synthesis inhibitor, cycloheximide (CHX), in the presence or absence of IMZ. HUVECs were treated with CHX 20 μ g/mL or IMZ 1 μ M + CHX 20 μ g/mL for 24 h. n = 8 per group. * P < .05 vs control. D, Western blot images and densitometric analysis of HIF-1 α in HUVECs treated with scrambled siRNA or HIF-1 α siRNA for 48 h. n = 4 per group. * P < .05 vs control. E, Representative images and dot-plot graph from the modified Boyden chamber migration assay. HIF-1 α knockdown or scramble siRNA-treated HUVECs were exposed to IMZ 1 μ M or vehicle control (water) for 16 h. Images were acquired at a magnification of 20 \times . Bar = 200 μ m. n = 4 per group. * P < .05 vs control, ^{##} P < .01 vs IMZ 1 μ M in control HUVECs. F, Representative images and dot-plot graph of quantification of network formation assay. HIF-1 α knockdown or control HUVECs were cultured in growth factor reduced Matrigel in the absence or presence of IMZ 1 μ M for 16 h. Images were acquired at a magnification of 10 \times . Network length was quantified by ImageJ software. Bar = 400 μ m. n = 4 per group. ** P < .01 vs control, ^{##} P < .01 vs IMZ 1 μ M in control HUVECs. G, Representative fluorescence images and fluorescence intensity of HUVECs treated with IMZ 1 μ M or vehicle control for 24 h, following by staining with HIF-1 α or DAPI. Fluorescence intensity was quantified using ImageJ software. Bar = 100 μ m. n = 4 per group. * P < .05 vs control. All data are presented as mean \pm SD. The statistical significance of the difference between the two groups was determined by the Mann-Whitney test. The statistical significance of the difference of more than 2 groups was determined by one-way ANOVA with Tukey's multiple comparison test

and FGF expression (Figure 5A). Taken together, our data suggest that HIF-1 α plays a crucial role in IMZ-induced angiogenesis in HUVECs.

3.4 | IMZ activates eNOS and increases NO production in HUVECs via activation of the PI3K/AKT pathway

Endothelium nitric oxide synthase (eNOS) plays a vital role in the maintenance of EC function and angiogenesis.²³ Upon activation by phosphorylation, eNOS catalyzes the conversion of L-arginine to nitric oxide (NO) and citrulline.²³ Since IMZ increased the angiogenic function of EC, we next determined the effects of IMZ on the eNOS/NO pathway. Multiple signaling pathways converge on the phosphorylation of serine 1177 to mediate eNOS activation.^{24,25} Exposure of HUVECs to IMZ (1 μ M) for 10 min resulted in a significant increase (~55%) in eNOS serine 1177 phosphorylation (Figure 4A). Intracellular NO was concomitantly monitored using a highly sensitive fluorescence dye, 4-amino-5-methylamino-2',7'-difluorofluorescein diacetate (DAF-FM DA). Consistent with the increased activation of eNOS, IMZ (1 μ M) significantly increased NO levels ~2.3 fold (Figure 4B). To assess the essentiality of eNOS in IMZ-induced augmentation of angiogenesis, we used a siRNA against eNOS (eNOS siRNA) to inhibit eNOS protein expression in HUVECs. eNOS was successfully knocked down by ~90% (Figure 4C) compared to scramble control. EC functional assays, including migration and network formation, were performed on eNOS siRNA transfected cells. eNOS siRNA significantly attenuated the increase in IMZ induced EC migration (Figure 4D) and network formation (Figure 4E). Notably, in eNOS deficient cells, the IMZ-induced increase of HIF-1 α protein expression was eliminated (Figure 4C), indicating that eNOS is indispensable for IMZ-induced increases in HIF-1 α . Moreover,

knockdown of HIF-1 α by siRNA did not alter eNOS expression levels (Figure 4F). Furthermore, in eNOS-deficient cells, the effects of IMZ on these proteins were completely blunted, suggesting that eNOS is crucial for the IMZ-induced increase of VEGF and FGF level (Figure 5B). Together, the data reveal that eNOS is a major contributor to IMZ-induced angiogenesis and responsible for increases in HIF-1 α protein. In addition, phosphatidylinositol 3-kinase (PI3K) and its downstream effector AKT are important for the activation of eNOS *via* phosphorylation at Ser1177.²⁶ In IMZ (1 μ M) treated HUVECs, there was a significant increase (~50%) in the phosphorylation of AKT at its full activation phosphorylation site, Ser473 compared to control (Figure 6A). A potent PI3K inhibitor, wortmannin (10 nM, 1-h pretreatment), completely abolished the ability of IMZ to activate AKT and eNOS (Figure 6B,C). There was no statistically significant difference in P-eNOS expression between IMZ and control-treated groups in the presence of wortmannin. These data suggest that IMZ activates eNOS through the PI3K/AKT signaling.

3.5 | IMZ enhances capillary formation in the subcutaneous Matrigel plug

To initially assess the ability of IMZ to induce angiogenesis in-vivo, we used the Matrigel Plug assay in adult male C57BL/6 mice. Ice-cold Matrigel solution (0.5 mL) supplemented with IMZ (1 μ M final concentration) or vehicle control (water) was injected subcutaneously into the mice. After 14 days, Matrigel plugs were collected. To visualize capillary density in the Matrigel plugs, we performed immunostaining against the endothelial marker, CD31. Capillary density was significantly higher in IMZ-containing plugs (~2.9 fold vs control plugs) (Figure 7A,B), demonstrating that IMZ significantly induced angiogenesis in vivo.

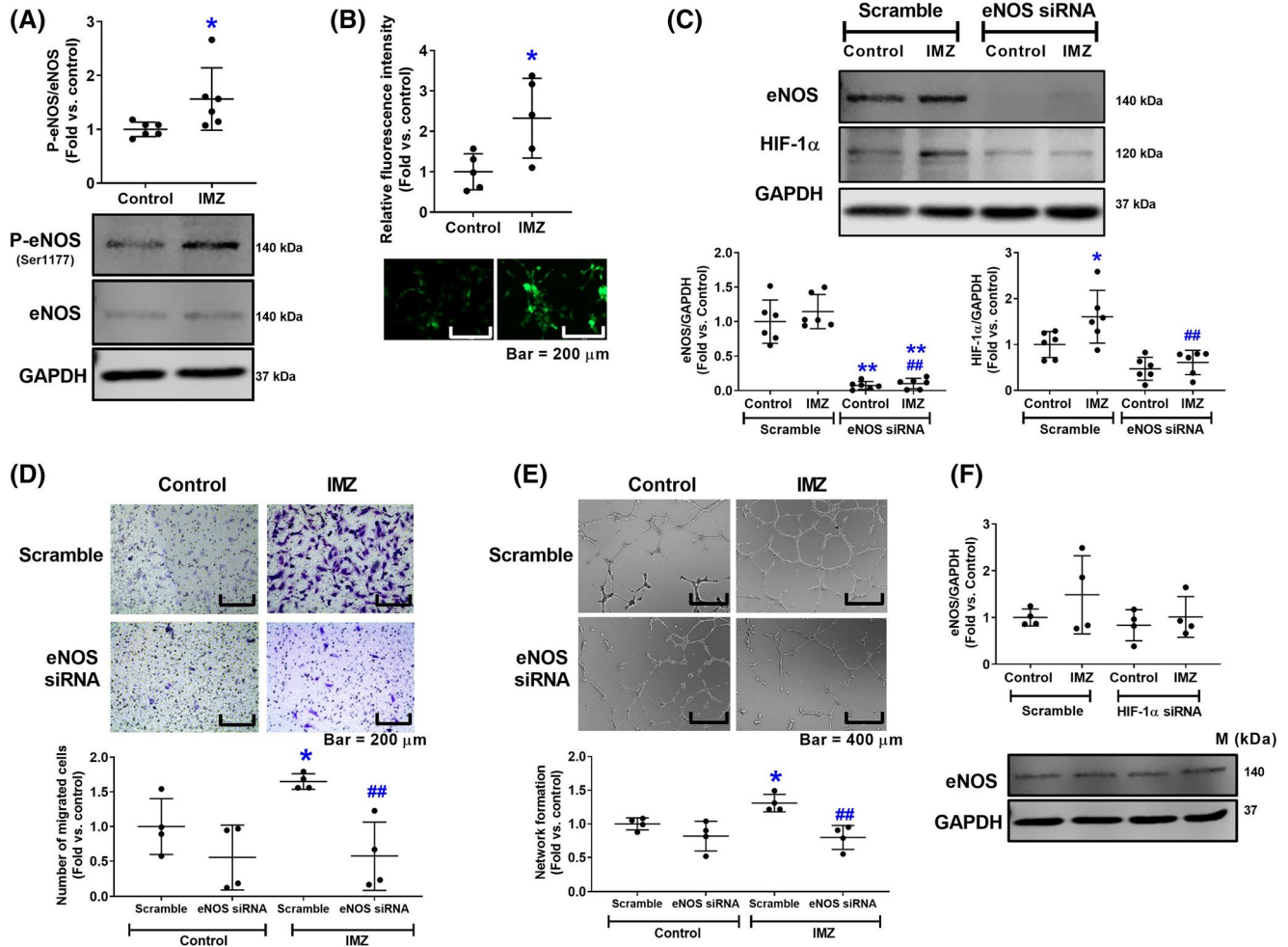


FIGURE 4 IMZ activates eNOS and increases Nitric Oxide production in HUVECs. A, Western blot images and densitometric analysis of P-eNOS (Ser1177) and eNOS in HUVECs treated with IMZ 1 μ M or vehicle control for 10 min. $n = 6$ per group. $*P < .05$ vs control. B, Representative fluorescence images and relative fluorescence intensity of HUVECs loaded with the NO sensitive dye, DAF-FM DA, in the presence or absence of IMZ 1 μ M. The fluorescence of the NO dye was examined using a fluorescent microscope (EVOS, Thermo Fisher Scientific) at an excitation wavelength of 480 nm and an emission of 510 nm. Fluorescence intensity was quantified using ImageJ software. $n = 5$ per group. $*P < .05$ vs control. C, Western blot images and densitometric analysis of eNOS and HIF-1 α expression levels. HUVECs were treated with eNOS siRNA or scramble siRNA for 48 h, followed by the exposure to IMZ 1 μ M or vehicle control for 24 h. $n = 6$ per group. $*P < .05$ vs scramble control, $**P < .01$ vs scramble control, $###P < .01$ vs IMZ in scramble. D, Representative images and dot-plot graph from the modified Boyden chamber migration assay. eNOS knockdown or control HUVECs were treated with IMZ 1 μ M or vehicle control (water) for 16 h. Images were taken at a magnification of 20 \times . Bar = 200 μ m. $n = 4$ per group. $*P < .05$ vs scramble control, $###P < .01$ vs IMZ in scramble. E, Representative images and dot-plot graph of the network formation assay. eNOS knockdown or control HUVECs were cultured in growth factor reduced Matrigel in the absence or presence of IMZ 1 μ M for 16 h. Images were taken under a magnification of 10 \times , and network length was quantified by ImageJ software. Bar = 400 μ m. $n = 4$ per group. $*P < .05$ vs scramble control, $###P < .01$ vs IMZ in scramble. F, Western blot images and densitometric analysis of eNOS expression level. HUVECs were treated with HIF-1 α siRNA or scramble siRNA for 48 h, followed by the exposure to IMZ 1 μ M or vehicle control for 24 h. $n = 4$ per group. All data are presented as mean \pm SD. The statistical significance of the difference between the two groups was determined by the Mann-Whitney test. The statistical significance of the difference of more than 2 groups was determined by one-way ANOVA with Tukey's multiple comparison test

3.6 | IMZ accelerates recovery from hind limb ischemia in hyperglycemic mice

Next, we evaluated the potential therapeutic efficacy of IMZ in a well-established animal model of hyperglycemia that exhibits delayed recovery from hind limb ischemia due to impaired angiogenesis.²⁷ Clinically, individuals with

hyperglycemia are at a much higher risk of developing critical limb ischemia to the extent that it might even require amputation.²⁸ Adult male C57BL/6J mice were rendered hyperglycemic by 5 consecutive low-dose (50 mg/kg) injections of streptozotocin (STZ). The wild type (WT) control mice received citrate buffer injections. Animals were kept for at least 3 months after confirmation of hyperglycemia

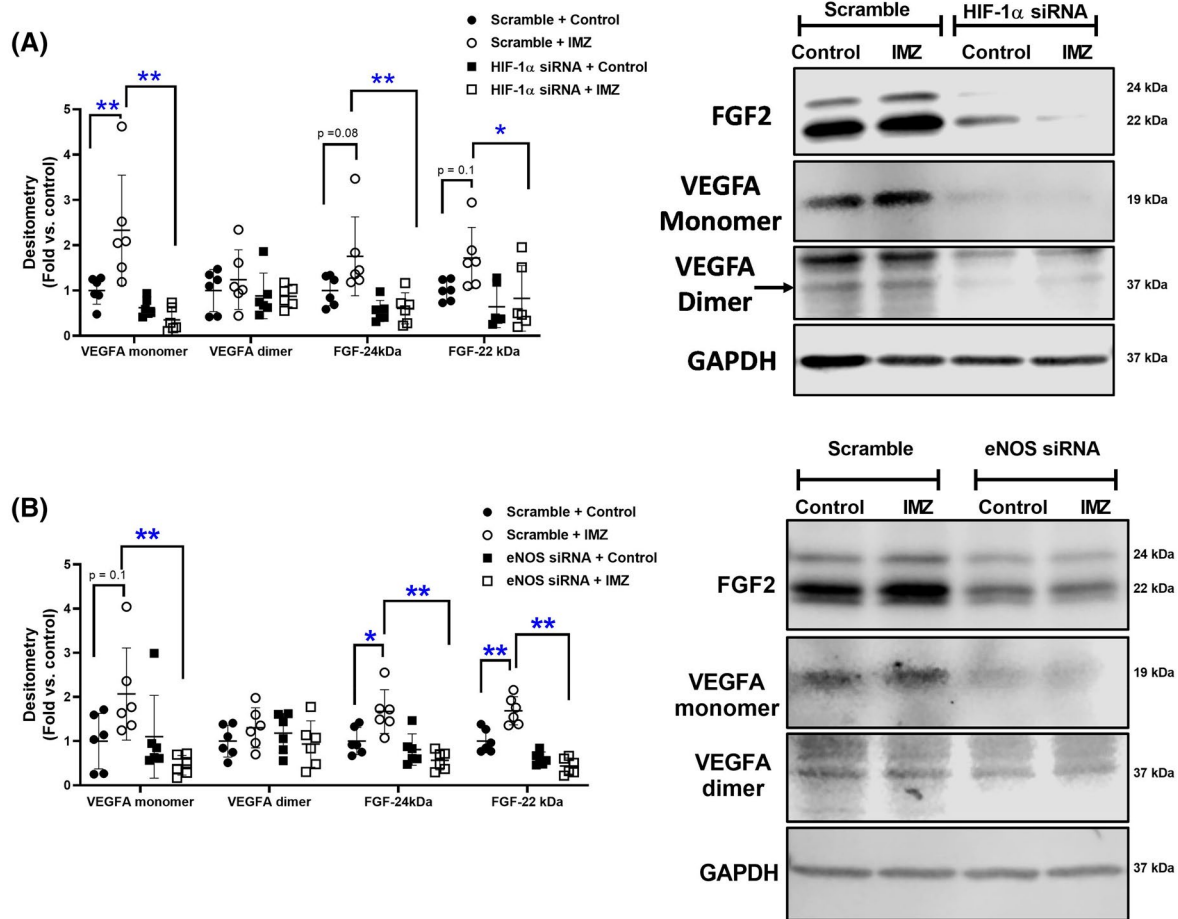


FIGURE 5 The effects of knocking down HIF-1 α and eNOS on IMZ-mediated expression of VEGFA and bFGF. A, Western blot images and densitometric analysis of bFGF and VEGFA expression level. HUVECs were treated with HIF-1 α siRNA or scramble siRNA for 48 h, followed by the exposure to IMZ 1 μ M or vehicle control for 24 h. $n = 6$ per group. $*P < .05$, $**P < .01$. B, Western blot images and densitometric analysis of bFGF and VEGFA expression level. HUVECs were treated with eNOS siRNA or scramble siRNA for 48 h, followed by the exposure to IMZ 1 μ M or vehicle control for 24 h. $n = 6$ per group. $*P < .05$, $**P < .01$. All data are presented as mean \pm SD. The statistical significance of the difference of more than 2 groups was determined by one-way ANOVA with Tukey's multiple comparison test

(≥ 250 mg/dL glucose, Figure 8B). Maintaining STZ-injected mice under hyperglycemia for 3 months allows our animal model to resemble chronic diabetic complications as seen in humans. Both WT and STZ mice received unilateral femoral artery ligation surgery, with the contralateral limb receiving sham surgery (artery isolation but no ligation). Animals were randomly divided into 4 groups: WT + PBS, WT + IMZ (20 mg/kg, ip twice/day), STZ + PBS, STZ + IMZ (20 mg/kg, ip, twice/day). Our pilot studies showed that IMZ at this dosage reached blood concentrations within the μ M range in C57B/6J mice (data not shown), comparable to the concentrations used in our in vitro studies. Furthermore, IMZ at this dosage exerted antidiabetic effects in type 2 diabetic mouse model, db/db mice, with no adverse effects (data not shown). There was no change in blood glucose or body weight between IMZ-treated STZ mice and control-treated STZ mice (Figure 8A,B). IMZ treatment did not affect blood glucose levels, as there was no difference in blood glucose between WT + PBS and WT + IMZ mice (Figure 8B). Blood

perfusion of the hind paw was assessed using a laser Doppler imaging system (Perimed) at different time points during the 21-day recovery (Figure 8C). The blood flow reperfusion in mouse paws depends on multiple factors such as ambient temperature, cardiac rhythm, and the deep of anesthesia, and so it varies at different time points. To accurately reflect the blood perfusion recovery, the limb receiving sham surgery was used as an internal control in each animal. The blood perfusion recovery index was calculated based on the blood perfusion in the ischemic paw divided by that in the sham paw. IMZ did not affect blood perfusion recovery in normoglycemic mice, as there was no difference between WT + PBS and WT + IMZ mice (Figure S6A). While the recovery of blood perfusion was significantly delayed in the STZ + PBS group compared with that in WT + PBS mice, there was no statistical difference between STZ + IMZ and WT + PBS over the post-surgery period of 21 days (Figure 8C,D). Two mice in the STZ + PBS group were euthanized prior to the end of the experiment due to significant toe/limb loss.

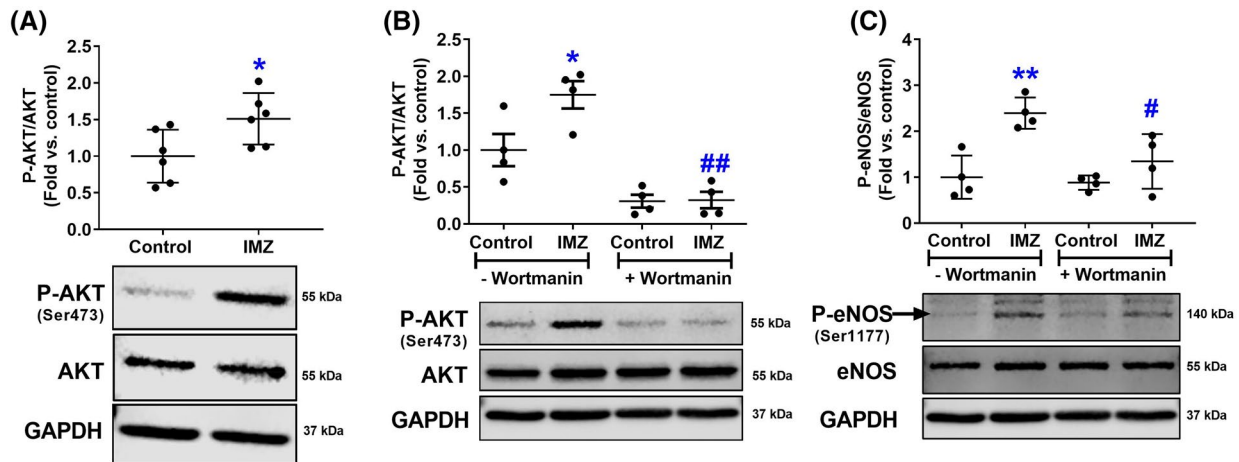


FIGURE 6 IMZ activates eNOS *via* PI3K/AKT signaling in HUVECs. A, Western blot images and densitometric analysis of P-AKT (ser473) and AKT in HUVECs treated with IMZ 1 μ M or vehicle control for 10 min. $n = 6$ per group. $*P < .05$ vs control. B, Western blot images and densitometric analysis of P-AKT (ser473) and AKT. HUVECs were pretreated with wortmannin (10 nM) for 1 h, followed by the addition of IMZ or vehicle (water) for 10 min. $n = 4$ per group. $*P < .05$ vs control, $##P < .01$ vs IMZ without wortmannin. C, Western blot images and densitometric analysis of P-eNOS (Ser1177) and eNOS. HUVECs were pretreated with wortmannin 10 nM for 1 h, followed by the addition of IMZ or vehicle (water) for 10 min. $n = 4$ per group. $**P < .01$ vs control, $#P < .05$ vs IMZ without wortmannin. All data are presented as mean \pm SD. The statistical significance of the difference between the two groups was determined by the Mann-Whitney test. The statistical significance of the difference of more than 2 groups was determined by one-way ANOVA with Tukey's multiple comparison test

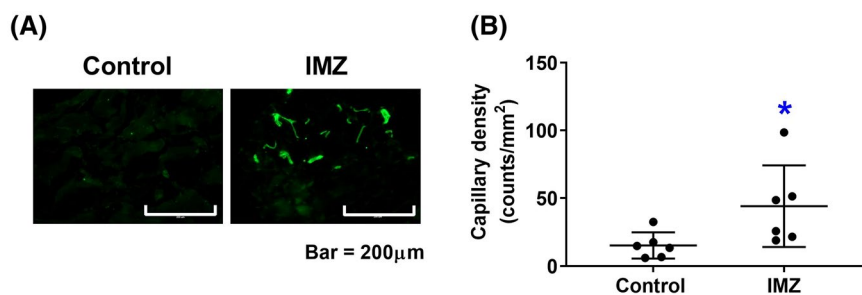


FIGURE 7 IMZ enhances capillary formation in the subcutaneous Matrigel plug assay. A, Representative images of Matrigel plugs stained with CD31. Matrigel plugs were collected 14-days post-injection, embedded in OCT, sectioned (10 μ m), and stained with antibody against the capillary marker, CD31. Bar = 200 μ m. B, Quantitation of capillary density of Matrigel plugs. $n = 6$ per group. $*P < .05$ vs control. All data are presented as mean \pm SD. The statistical significance of the difference between the two groups was determined by the Mann-Whitney test

In contrast, in the STZ + IMZ group, there was a significantly accelerated recovery in blood perfusion compared to that in the STZ + PBS group, as early as the 7th day post-surgery, and which continued throughout the recovery period (Figure 8C). To further evaluate the effects of IMZ on neovascularization in ischemic limbs, we assessed the number of capillary-like structures by CD31 staining in ischemic muscles collected at the end of the study (21-day post-surgery). Capillary density was significantly lower in STZ + PBS mice than in WT + PBS mice, whereas STZ + IMZ mice had significantly higher capillary density than in STZ + PBS mice (Figure 8E). Interestingly, similar results were observed in hind limb ischemic mice treated with IMZ for 7 days, suggesting that the effects of IMZ on the formation of capillaries occurs within the first 7 days (Figure S6B). Because lowering

the incidence of necrosis is important for the management of diabetic microangiopathy,²⁹ we recorded tissue necrosis during the experiment. There were 2 incidences of necrosis within the STZ + PBS group (40%), and no necrosis in WT + PBS and STZ + IMZ groups (Figure 8F), suggesting administration of IMZ protected ischemic tissue from necrosis in the context of hyperglycemia. Western blot analysis of ischemic muscles on 21-day post-surgery revealed a nearly 40% decrease of P-AKT in the STZ + PBS mice compared with that in WT + PBS mice, whereas P-AKT was significantly increased in STZ + IMZ mice compared to STZ + PBS controls (Figure 8G). In addition, while there were ~70% and 60% reductions in the expression of HIF-1 α and P-eNOS, respectively, in STZ + PBS mice compared to that in WT mice, IMZ treatment increased ~25% of each of the two

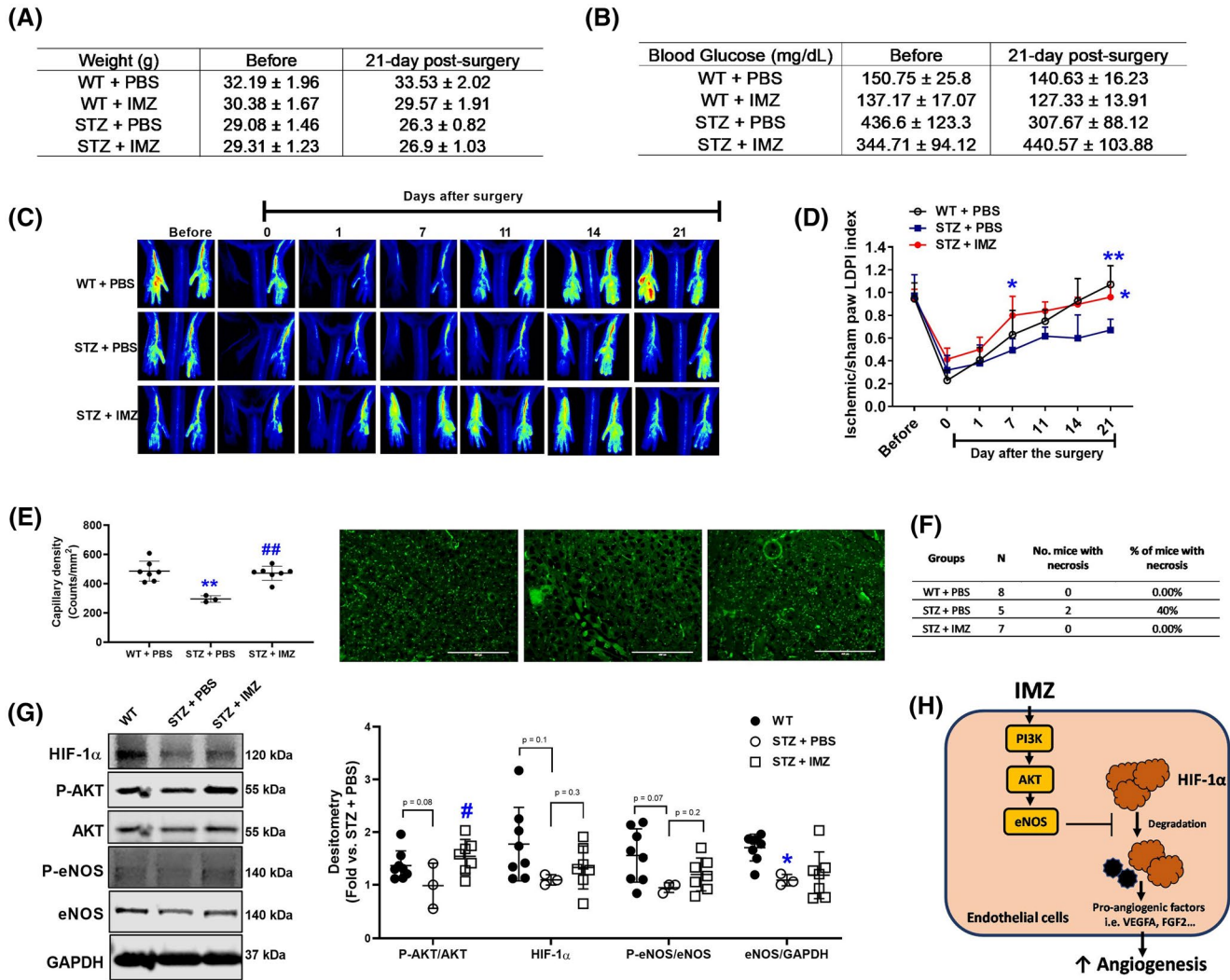


FIGURE 8 IMZ accelerates recovery from hind limb ischemia in hyperglycemic mice. A, Table of body weight of mice measured before and 21-day after surgery. WT + PBS (n = 8), WT + IMZ (n = 6), STZ + PBS (n = 5), STZ + IMZ (n = 7). B, Table of blood glucose taken from the tail vein of WT + PBS (n = 8), WT + IMZ (n = 6), STZ + PBS (n = 5), STZ + IMZ (n = 7). Blood glucose was determined with a blood glucose meter. C, Representative images of hind-limb blood perfusion at various time points. Blood perfusion was recorded with a laser Doppler imaging system. WT + PBS (n = 8), STZ + PBS (n = 7), STZ + IMZ (n = 7). D, Quantitation of the blood perfusion recovery index at various time points. The blood perfusion recovery index is represented as the ratio of blood perfusion in the ischemic paw relative to the sham paw. * $P < .05$ STZ + IMZ vs STZ + PBS. ** $P < .01$ WT + PBS vs STZ + PBS. E, Representative images and quantitation of the capillary density of ischemic muscle sections stained with CD31. Ischemic muscles were collected at the end of the study (21-day post-surgery). Ischemic muscles were fixed with 4% PFA, embedded in OCT, sectioned (8 μ m), and stained with CD31. Bar = 400 μ m. ** $P < .01$ vs WT + PBS, ### $P < .01$ vs STZ + PBS. F, Incidence of tissue necrosis in each group of mice. G, Western blot images and densitometric analysis of P-AKT (ser473), AKT, HIF-1 α , P-eNOS (ser1177), eNOS in ischemic muscles of WT (n = 8), STZ + PBS (n = 3) or STZ + IMZ (n = 7) mice. * $P < .05$ vs WT, # $P < .05$ vs STZ + PBS (H) Schema of IMZ's proposed signaling pathway. All data are presented as the mean \pm SD. The statistical significance of the difference in more than 2 groups was determined by one-way ANOVA with Tukey's multiple comparison test. For laser Doppler blood perfusion data, two-way repeated-measures ANOVA followed by Bonferroni's multiple comparison test was used

proteins compared to PBS treated diabetic mice (Figure 8G). Together, this data suggests AKT/eNOS/HIF-1 α axis is concomitantly activated upon IMZ treatment in ischemia. In addition, there was a significant decrease in VEGFA dimer expression levels in the STZ + PBS mice compared with that in WT + PBS mice, whereas VEGFA levels were modestly higher in STZ + IMZ mice compared to STZ + PBS controls ($P = .26$). There were no differences in either isoforms

of FGF between IMZ treated and PBS treated diabetic mice (Figure S7). We speculate that the much smaller changes in VEGF and FGF in the in vivo study might be due to the small sample size (n = 3) and the fact that the levels of these two growth factors in skeletal muscles might have masked their changes in ECs within the tissue. Taken together, these data illustrate that treatment with IMZ accelerates post-ischemic revascularization in hyperglycemic mice, and the AKT/

eNOS/HIF-1 α axis is involved in IMZ induced angiogenesis in the hind limb ischemic mouse model.

4 | DISCUSSION

The novel imidazolinone metabolite of metformin, IMZ, was identified as the product of the scavenging of MG by metformin in patients with type-2 diabetes.⁸ Although IMZ possesses an imidazolinone functional group, the biological properties of IMZ remain unknown. We now demonstrate the pro-angiogenic properties of IMZ and the signaling pathways engaged by IMZ. At relatively low concentrations, IMZ enhanced EC migration and network formation in vitro (Figure 1), with a concomitant increase in several intracellular and secreted pro-angiogenic factors, such as VEGFA and bFGF (Figure 2). We further demonstrated that eNOS/HIF-1 α plays an indispensable role in IMZ-induced angiogenesis in vitro (Figures 3 and 4). The induction of angiogenesis by IMZ was further confirmed in vivo with the Matrigel plug assay (Figure 7). Importantly, in a chronic hyperglycemic mouse model with impaired angiogenesis, IMZ treatment significantly accelerated neovascularization from hind limb ischemia and reduced tissue necrosis (Figure 8). Our work has unveiled the pro-angiogenic effects of IMZ, its underlying signaling pathways via eNOS/HIF-1 α (Figure 8H), and contributes to the development of potential pro-angiogenic agents for the treatment of PAD.

HIF-1 α signaling is one of the most potent pathways in regulating angiogenesis.¹³ Although HIF-1 α is stabilized during hypoxia,¹² the regulatory mechanism of HIF-1 α signaling under normoxic conditions is not fully understood. The HIF-1 α protein abundance appears to be regulated at different levels. At the transcriptional level, activation of the PI3K/AKT pathway leads to phosphorylation of the eukaryotic translation initiation factor 4E (eIF-4E), which is essential for inhibiting cap-dependent mRNA translation, resulting in enhanced HIF-1 α protein translation.³⁰ IMZ was shown to activate the PI3K/AKT pathway (Figure 6). However, there was no change in eIF-4E phosphorylation (Figure S8A) or HIF-1 α mRNA levels (Figure 3B) upon IMZ treatment, suggesting a non-canonical pathway is engaged during IMZ-induced HIF-1 α upregulation. Furthermore, eNOS is phosphorylated at Ser1177 by IMZ, with a concomitant increase in NO production (Figure 4A,B). IMZ mediated NO production is not associated with the inflammatory process as there was no difference in inflammatory markers such as iNOS, VCAM-1 or ICAM-1, between control and IMZ treated HUVECs (Figure S8B). Furthermore, levels of potential endotoxin contamination, which is known to induce angiogenesis, in IMZ samples were below the limits of detection (Figure S9). In addition, eNOS is required for IMZ-mediated upregulation of HIF-1 α (Figure 4C). Although the

roles of NOS isoforms in regulating HIF-1 α are not well established, studies have demonstrated the importance of the eNOS/NO axis in HIF-1 α stabilization and activation.³¹ NO is known to stabilize HIF-1 α via three putative mechanisms: (a) Directly modifying HIF-1 α through S-nitrosylation³²; (b) activating PI3K/AKT and MAPK pathways³³; and (c) impairing HIF-1 α degradation by inhibition of prolyl hydroxylases.³⁴ The mechanism(s) by which IMZ interacts with eNOS/HIF-1 α regulatory networks warrants further investigation.

Multiple mechanisms, including transcription, translation, post-translational modification, and protein-protein interaction, are known to regulate HIF-1 α levels. Among these, post-translational modifications, such as hydroxylation, ubiquitination, S-nitrosylation, phosphorylation, and acetylation, have been shown to influence the half-life and/or transcriptional activity of HIF-1 α .³⁵ Our work showed that IMZ did not affect HIF-1 α phosphorylation or prolyl hydroxylases (PHD)-mediated hydroxylation (Figure S5B). Several studies have suggested the involvement of direct post-translational modification of HIF-1 α via S-nitrosylation, particularly in NO-mediated HIF-1 α activation.³⁶⁻³⁹ Some critical cysteine residues of HIF-1 α were demonstrated to be susceptible with S-nitrosylation. For example, the S-nitrosoglutathione-mediated prevention of HIF-1 α degradation is dependent on the S-nitrosylation of Cys533 in HIF-1 α in 4T1 cells.³² S-nitrosylation of Cys800 in HIF-1 α has been associated with an increase in interaction of HIF-1 α with p300, thus enhancing its transcriptional activity.⁴⁰ Our study showed that IMZ increases NO production in endothelial cells (Figure 4B). We speculated that IMZ might be able to stabilize HIF-1 α via S-nitrosylation, but further works are needed to determine the exact mechanism for HIF-1 α post-translation modifications, especially S-nitrosylation by IMZ.

Diabetes is a chronic metabolic disorder that affects 1 in 10 Americans.⁴¹ One of the most devastating complications of diabetes is PAD, which, in its severest form, causes critical limb ischemia due to impaired neovascularization.⁴² Therapeutic strategies designed to improve angiogenesis have been the subject of intensive research. However, no small molecule with satisfactory efficacy exists that enhances new blood vessel formation. Indeed, most of the pro-angiogenic therapies have primarily focused on the administration of growth factors such as VEGFA and bFGF, or the delivery of stem/progenitor cells, but these are currently considered only modestly successful and can be accompanied by multiple adverse effects.⁴³⁻⁴⁵ Consequently, there is a need to discover novel small molecules for the treatment of PAD. Herein, we provide evidence that IMZ accelerates blood flow recovery (Figure 8C,D), muscle revascularization (Figure 8E), and protects against tissue necrosis (Figure 8F) in a diabetic mouse model. The ability to accelerate blood flow may be useful in preventing and reducing the severity of

acute ischemic episodes, particularly in diabetic patients at a high risk of developing PAD.

MG is highly elevated in hypertensive and diabetic patients and is widely recognized as a major contributor to cellular damage and dysfunction.⁶ MG is also the major precursor to advanced glycation end products, which exacerbate both oxidative stress and inflammation, further contributing to tissue damage.^{46,47} Some MG adducts exhibit pharmacological activity^{48,49} and since IMZ is formed from the adduction of MG with metformin, its potential biological properties warrant investigation. The structure of IMZ includes an imidazoline/guanidine functional group. Indeed, many compounds containing imidazoline/guanidine groups, such as arginine and agmatine, are important in treating fungal infections,⁵⁰ hypertension⁵¹ and cardiovascular disease.⁵² Arginine is known to improve endothelial dysfunction in patients with essential hypertension.¹⁰ Arginine increases EC function by enhancing the AKT/eNOS/NO pathway.⁹ Our finding that IMZ improves EC angiogenesis and protected hyperglycemic mice from hind limb ischemia provides further evidence for its therapeutic potential. Structure-activity studies are required for a better understanding of the application of imidazoline/guanidine-based small molecules in the treatment of diabetic cardiovascular complications.

Metformin is well known to improve endothelial cell function and to alleviate cardiovascular complications; however, the effects of metformin on angiogenesis remain controversial depending on disease models and cellular environmental conditions. While metformin is anti-angiogenic in some cancer models, it improves angiogenesis in hyperglycemic mice.⁵³ Metformin inhibits network formation in HUVECs cultured in normal glucose,⁵⁴ while, at an equivalent dose, exerted opposing effects under hyperglycemic conditions.⁵³ We speculate that the gradual accumulation of a large amount of MG upon exposure to hyperglycemia can be scavenged by metformin, resulting in IMZ formation. Therefore, the paradoxical effects of metformin on EC function might actually depend on the IMZ concentrations in the experimental system. We further speculate that although IMZ is a scavenged product of metformin, it owns characteristics that are distinct from metformin, because IMZ exerts pro-angiogenesis effects at relatively low concentrations (μM) compared to that of metformin (mM). Further work on how IMZ contributes to the mechanism of action of metformin is in compelling need.

Finally, there are several limitations of the study. First, although our data strongly suggest that HIF-1 α and eNOS mediate the angiogenic effects of IMZ *in vitro*, we cannot exclude the possibility that other proangiogenic factors, such as VEGFA and bFGF contribute to the angiogenic response to IMZ. Secondly, in the *in vivo* Matrigel plug assay, IMZ is delivered locally within the Matrigel. The subsequent neovascularization occurs mainly via the infiltration of resident cells such as ECs, monocytes, and macrophages

into the Matrigel plugs. However, angiogenesis is a complex process, in which both pro- and anti-angiogenic factors can influence the angiogenic response.⁵⁵ Given that IMZ mediates its effects *via* downstream angiogenesis signaling, conditioned medium from IMZ-treated cells should be examined. Thirdly, wortmannin was used to inhibit PI3K. However, because pharmacological inhibitor might have off-target effects, the roles of PI3K/AKT in IMZ induced angiogenesis remain to be elucidated using complementary genetic approaches. We understand that arterial endothelial cells are more clinically relevant than HUVECs to study angiogenesis. Although HUVECs do not represent all endothelial cell types found in an organism, they are the most well-established model for the study of vascular endothelium properties and the main biological pathways involved in endothelium function, including angiogenesis. However, the vein endothelial cells are different from arterial endothelial cells in morphology and function.⁵⁶ For example, while venular endothelial cells are the primary sites for immune cell trafficking, arteriolar endothelial cells robustly control vascular tone.⁵⁶ Therefore, it is important to observe the impact of IMZ on angiogenesis using different endothelial cell models such as arterial endothelial cells. In addition, since C57B/6J mice are more amputation resistance than mice with other genetic backgrounds, additional mouse models could also be used to investigate the effects of IMZ on angiogenesis *in vivo*. The effects of IMZ on angiogenesis *in vivo* should ideally be examined using expanded sample size and models of diabetes, such as the diet-induced obese (DIO) mouse, and Zucker diabetic fatty (ZDF) rats. Though the concentration and doses of IMZ used in this study were chosen based on our prior observations of patient urine, the range of IMZ in plasma of metformin-treated diabetic patients remains to be determined. Since IMZ was detected in T2D patients taking MF, the level of IMZ in biological samples is an attractive question. A multiple reaction monitoring (MRM) method was developed in our laboratory to specifically look at the level of IMZ in urine samples.⁸ Urine was chosen due to the reduced complexity of the matrix and presumed higher concentrations of IMZ. IMZ was detected at the level of 18.8 nM to 4.3 μM after taking into account the detection limit of the mass spectrum and the dilution factors of urine samples.⁸ Although no conclusive data yet, we were able to detect IMZ in one plasma sample from the patient with the highest IMZ concentration in the urine, suggesting the feasibility of IMZ detection in other biological specimens such as plasma. Further studies are needed to access plasma concentrations of IMZ in patients receiving metformin. Our findings have shown that IMZ increases EC angiogenesis and protects hyperglycemic mice from hind limb ischemia, suggesting the therapeutic potential of IMZ at μM concentrations. We believe that it is particularly compelling to dissect the role of IMZ on diabetic cardiovascular

complications at the physiological levels in diabetic patients once the information of IMZ concentrations in plasma has been acquired. In addition, future studies are needed to determine whether IMZ can rescue hyperglycemia-induced EC dysfunction and the effects of high glucose on IMZ-induced eNOS/HIF-1 signaling pathway in vitro. The effects of IMZ on downstream pro-angiogenic mediators such as VEGF and FGF could also be examined using eNOS knock out mice. By uncovering IMZ's biological properties and signaling, our work has important implications for the development of novel therapeutic strategies to rescue impairments in angiogenesis under diabetic conditions.

ACKNOWLEDGMENT

We would like to thank Dr Steve Firestone at the Department of Pharmaceutical Sciences, Eugene Applebaum College of Pharmacy and Health Sciences, Wayne State University, MI, USA, for assisting us with NMR and MS analysis. We also thank the staff from the Department of Laboratory Animal Research at Wayne State University for providing excellent care for the animals.

DISCLOSURES

No conflicts of interest, financial or otherwise, are declared by the authors.

AUTHOR CONTRIBUTIONS

H. Nguyen conducted experiments, acquired data, analyzed data, and wrote the manuscript; J.Y. Koh conducted experiments, acquired data, and edited the manuscript; H. Li conducted experiments and edited the manuscript. A. Islas-Robles conceived the idea and edited the manuscript; S.P. Meda Venkata conducted experiments and edited the manuscript; J.-M. Wang and T.J. Monks conceived the idea, designed research studies, analyzed data, edited the manuscript, and provided research funding. J.-M. Wang and T.J. Monks are the guarantors of this work and, as such, had full access to all the data in the study and assume responsibility for the integrity of the data and the accuracy of data analysis.

DATA AVAILABILITY STATEMENT

The datasets and resources in this study are available from the corresponding author upon reasonable request.

REFERENCES

- Peripheral arterial disease in people with diabetes. *Diabetes Care*. 2003;26(12):3333-3341. <https://doi.org/10.2337/diacare.26.12.3333>.
- Mohler ER. Therapy insight: peripheral arterial disease and diabetes—from pathogenesis to treatment guidelines. *Nat Clin Pract Cardiovasc Med*. 2007;4(3):151-162. <https://doi.org/10.1038/ncpcardio0823>.
- Uccioli L, Meloni M, Izzo V, Giurato L, Merolla S, Gandini R. Critical limb ischemia: current challenges and future prospects. *Vasc Heal Risk Manag*. 2018;14:63-74. <https://doi.org/10.2147/vhrm.s125065>.
- Annex BH. Therapeutic angiogenesis for critical limb ischaemia. *Nat Rev Cardiol*. 2013;10:387-396.
- Iyer SR, Annex BH. Therapeutic angiogenesis for peripheral artery disease. *JACC: Basic Transl Sci*. 2017;2(5):503-512. <https://doi.org/10.1016/j.jacbs.2017.07.012>.
- Nigro C, Leone A, Raciti GA, et al. Methylglyoxal-glyoxalase 1 balance: the root of vascular damage. *Int J Mol Sci*. 2017;18(1):188.
- Ruggiero-Lopez D, Lecomte M, Moinet G, Patereau G, Lagarde M, Wiernsperger N. Reaction of metformin with dicarbonyl compounds. Possible implication in the inhibition of advanced glycation end product formation. *Biochem Pharmacol*. 1999;58:1765-1773.
- Kinsky OR, Hargraves TL, Anumol T, et al. Metformin scavenges methylglyoxal to form a novel imidazolone metabolite in humans. *Chem Res Toxicol*. 2016;29:227-234.
- Joshi MS, Ferguson TB, Johnson FK, Johnson RA, Parthasarathy S, Lancaster JR. Receptor-mediated activation of nitric oxide synthesis by arginine in endothelial cells. *Proc Natl Acad Sci*. 2007;104(24):9982-9987. <https://doi.org/10.1073/pnas.0506824104>.
- Lekakis JP, Papathanassiou S, Papaioannou TG, et al. Oral L-arginine improves endothelial dysfunction in patients with essential hypertension. *Int J Cardiol*. 2002;86:317-323.
- El-Awady MS, Suddek GM. Agmatine ameliorates atherosclerosis progression and endothelial dysfunction in high cholesterol-fed rabbits. *J Pharm Pharmacol*. 2014;66(6):835-843. <https://doi.org/10.1111/jphp.12204>.
- Lee J-W, Bae S-H, Jeong J-W, Kim S-H, Kim K-W. Hypoxia-inducible factor (HIF-1) α : its protein stability and biological functions. *Exp Mol Med*. 2004;36(1):1-12. <https://doi.org/10.1038/emmm.2004.1>.
- Krock BL, Skuli N, Simon MC. Hypoxia-induced angiogenesis: good and evil. *Genes Cancer*. 2011;2(12):1117-1133. <https://doi.org/10.1177/1947601911423654>.
- Tang N, Wang L, Esko J, et al. Loss of HIF-1 α in endothelial cells disrupts a hypoxia-driven VEGF autocrine loop necessary for tumorigenesis. *Cancer Cell*. 2004;6:485-495.
- Treins C, Giorgetti-Peraldi S, Murdaca J, Semenza GL, Van Obberghen E. Insulin stimulates hypoxia-inducible factor 1 through a phosphatidylinositol 3-kinase/target of rapamycin-dependent signaling pathway. *J Biol Chem*. 2002;277(31):27975-27981. <https://doi.org/10.1074/jbc.m204152200>.
- Olson N, van der Vliet A. Interactions between nitric oxide and hypoxia-inducible factor signaling pathways in inflammatory disease. *Nitric Oxide*. 2011;25(2):125-137. <https://doi.org/10.1016/j.niox.2010.12.010>.
- Wang J-M, Tao J, Chen D-D, et al. MicroRNA miR-27b rescues bone marrow-derived angiogenic cell function and accelerates wound healing in type 2 diabetes mellitus. *Arterioscler Thromb Vasc Biol*. 2014;34(1):99-109. <https://doi.org/10.1161/atvbaaha.113.302104>.
- Li H, Liu J, Wang Y, et al. MiR-27b augments bone marrow progenitor cell survival via suppressing the mitochondrial apoptotic pathway in Type 2 diabetes. *Am J Physiol Endocrinol Metab*. 2017;313(4):E391-E401. <https://doi.org/10.1152/ajpen.0.00073.2017>.

19. Bandyopadhyay A, Zhu Y, Malik SN, et al. Extracellular domain of TGF β type III receptor inhibits angiogenesis and tumor growth in human cancer cells. *Oncogene*. 2002;21(22.), 3541-3551. <https://doi.org/10.1038/sj.onc.1205439>.
20. Tamarat R, Silvestre JS, Durie M, Levy BI. Angiotensin II angiogenic effect in vivo involves vascular endothelial growth factor- and inflammation-related pathways. *Lab Invest*. 2002;82:747-756.
21. Zhu Z, Zhong H, Zhou Q, et al. Inhibition of PKR impairs angiogenesis through a VEGF pathway. *Am J Physiol Endocrinol Metab*. 2015;308(6):E518-E524. <https://doi.org/10.1152/ajpen.00469.2014>.
22. Ucuzian AA, Gassman AA., East AT, Greisler HP. Molecular mediators of angiogenesis. *J Burn Care Res*. 2010;31(1):158-175. <https://doi.org/10.1097/bcr.0b013e3181c7ed82>.
23. Bir SC, Xiong Y, Kevil CG, Luo J. Emerging role of PKA/eNOS pathway in therapeutic angiogenesis for ischaemic tissue diseases. *Cardiovasc Res*. 2012;95:7-18.
24. Chen Z-P, Mitchelhill KI, Michell BJ, et al. AMP-activated protein kinase phosphorylation of endothelial NO synthase. *FEBS Letters*. 1999;443(3), 285-289. [https://doi.org/10.1016/s0014-5793\(98\)01705-0](https://doi.org/10.1016/s0014-5793(98)01705-0).
25. Boo YC, Sorescu G, Boyd N, et al. Shear stress stimulates phosphorylation of endothelial nitric-oxide synthase at Ser1179 by Akt-independent mechanisms. *J Biol Chem*. 2002;277(5):3388-3396. <https://doi.org/10.1074/jbc.m108789200>.
26. Dimmeler S, Fleming I, Fisslthaler B, Hermann C, Busse R, Zeiher AM. Activation of nitric oxide synthase in endothelial cells by Akt-dependent phosphorylation. *Nature*. 1999;399(6736):601-605. <https://doi.org/10.1038/21224>.
27. Couffignal T, Silver M, Zheng LP, Kearney M, Witzensbichler B, Isner JM. Mouse model of angiogenesis. *Am J Pathol*. 1998;152:1667-1679.
28. Thiruvoipati T, Kielhorn CE, Armstrong EJ. Peripheral artery disease in patients with diabetes: epidemiology, mechanisms, and outcomes. *World J Diabetes*. 2015;6:961-969.
29. Edmonds M. Diabetic foot ulcers. *Drugs*. 2006;66:913-929.
30. Masoud GN, Li W. HIF-1 α pathway: role, regulation and intervention for cancer therapy. *Acta Pharm Sin B*. 2015;5:378-389.
31. Schleicher M, Yu J, Murata T, et al. The Akt1-eNOS axis illustrates the specificity of kinase-substrate relationships in vivo. *Sci Signal*. 2009;2(82):ra41.
32. Li F, Sonveaux P, Rabbani ZN, et al. Regulation of HIF-1 α stability through S-nitrosylation. *Mol Cell*. 2007;26:63-74.
33. Kasuno K, Takabuchi S, Fukuda K, et al. Nitric oxide induces hypoxia-inducible factor 1 activation that is dependent on MAPK and phosphatidylinositol 3-kinase signaling. *J Biol Chem*. 2004;279:2550-2558.
34. Metzen E, Zhou J, Jelkmann W, Fandrey J, Brüne B. Nitric oxide impairs normoxic degradation of HIF-1 α by inhibition of prolyl hydroxylases. *Mol Biol Cell*. 2003;14:3470-3481.
35. Brahimi-Horn C, Mazure N, Pouyssegur J. Signalling via the hypoxia-inducible factor-1 α requires multiple posttranslational modifications. *Cell Signal*. 2005;17:1-9.
36. Palmer LA, Gaston B, Johns RA. Normoxic stabilization of hypoxia-inducible factor-1 expression and activity: redox-dependent effect of nitrogen oxides. *Mol Pharmacol*. 2000;58:1197-1203.
37. Bove PF, Hristova M, Wesley UV, Olson N, Lounsbury KM, van der Vliet A. Inflammatory levels of nitric oxide inhibit airway epithelial cell migration by inhibition of the kinase ERK1/2 and activation of hypoxia-inducible factor-1 α . *J Biol Chem*. 2008;283:17919-17928.
38. Park YK, Ahn DR, Oh M, et al. Nitric oxide donor, (+/-)-S-nitroso-N-acetylpenicillamine, stabilizes transactive hypoxia-inducible factor-1 α by inhibiting von Hippel-Lindau recruitment and asparagine hydroxylation. *Mol Pharmacol*. 2008;74:236-245.
39. Wang F, Sekine H, Kikuchi Y, et al. HIF-1 α -prolyl hydroxylase: molecular target of nitric oxide in the hypoxic signal transduction pathway. *Biochem Biophys Res Comm*. 2002;295:657-662.
40. Yasinska IM, Sumbayev VV. S-nitrosation of Cys-800 of HIF-1 α protein activates its interaction with p300 and stimulates its transcriptional activity. *FEBS Lett*. 2003;549:105-109.
41. Grundy SM, Benjamin JJ, Burke GL, et al. Diabetes and cardiovascular disease. *Circulation*. 1999;100:1134-1146.
42. Marso SP, Hiatt WR. Peripheral arterial disease in patients with diabetes. *J Am Coll Cardiol*. 2006;47:921-929.
43. Stewart DJ, Kutryk MJ, Fitchett D, et al. VEGF gene therapy fails to improve perfusion of ischemic myocardium in patients with advanced coronary disease: results of the NORTHERN trial. *Mol Ther*. 2009;17:1109-1115.
44. Simons M, Annex BH, Laham RJ, et al. Pharmacological treatment of coronary artery disease with recombinant fibroblast growth factor-2: double-blind, randomized, controlled clinical trial. *Circulation*. 2002;105:788-793.
45. Ripa RS, Wang Y, Jorgensen E, Johnsen HE, Hesse B, Kastrup J. Intramyocardial injection of vascular endothelial growth factor-A165 plasmid followed by granulocyte-colony stimulating factor to induce angiogenesis in patients with severe chronic ischaemic heart disease. *Eur Heart J*. 2006;27:1785-1792.
46. Ramasamy R, Yan SF, Schmidt AM. Methylglyoxal comes of AGE. *Cell*. 2006;124:258-260.
47. Davies SS, Zhang LS. Reactive carbonyl species scavengers-novel therapeutic approaches for chronic diseases. *Curr Pharmacol Rep*. 2017;3:51-67.
48. Zhou Q, Gong J, Wang M. Phloretin and its methylglyoxal adduct: Implications against advanced glycation end products-induced inflammation in endothelial cells. *Food Chem Toxicol*. 2019;129:291-300.
49. Cui H, Tao F, Hou Y, et al. Dual effects of propyl gallate and its methylglyoxal adduct on carbonyl stress and oxidative stress. *Food Chem*. 2018;265:227-232.
50. Bogle RG, Whitley GS, Soo SC, Johnstone AP, Vallance P. Effect of anti-fungal imidazoles on mRNA levels and enzyme activity of inducible nitric oxide synthase. *Br J Pharmacol*. 1994;111:1257-1261.
51. Fenton C, Keating GM, Lyseng-Williamson KA. Moxonidine. *Drugs*. 2006;66:477-496.
52. Raasch W, Schäfer U, Chun J, Dominiak P. Biological significance of agmatine, an endogenous ligand at imidazoline binding sites. *Br J Pharmacol*. 2001;133:755-780.
53. Yu J-W, Deng Y-P, Han X, Ren G-F, Cai J, Jiang G-J. Metformin improves the angiogenic functions of endothelial progenitor cells via activating AMPK/eNOS pathway in diabetic mice. *Cardiovasc Diabetol*. 2016;15:88.
54. Esfahanian N, Shakiba Y, Nikbin B, et al. Effect of metformin on the proliferation, migration, and MMP-2 and -9 expression of human umbilical vein endothelial cells. *Mol Med Rep*. 2012;5:1068-1074.

55. Norrby K. In vivo models of angiogenesis. *J Cell Mol Med.* 2006;10:588-612.
56. dela Paz NG, D'Amore PA. Arterial versus venous endothelial cells. *Cell Tissue Res.* 2009;335:5-16.

SUPPORTING INFORMATION

Additional Supporting Information may be found online in the Supporting Information section.

How to cite this article: Nguyen H, Koh JY, Li H, et al. A novel imidazolinone metformin-methylglyoxal metabolite promotes endothelial cell angiogenesis via the eNOS/HIF-1 α pathway. *The FASEB Journal.* 2021;35:e21645. <https://doi.org/10.1096/fj.202002674RR>